Journal of Applied Fluid Mechanics, Vol. 18, No. 4, pp. 976-991, 2025.
Available online at www.jafmonline.net, ISSN 1735-3572, EISSN 1735-3645.
https://doi.org/10.47176/jafm.18.4.3019

Numerical Study on Aerodynamic Characteristics of H-Darrieus Wind Turbine with Blunt Trailing-edge Airfoil

Z. Kong and X. Sun†

School of Energy and Power Engineering, University of Shanghai for Science and Technology, Shanghai, 200093, PR China

†Corresponding email: xjsun@usst.edu.cn

ABSTRACT

The present study numerically examines the aerodynamic performance of an H-type vertical axis wind turbine (VAWT) utilizing airfoils with blunt trailing edges (BTE). A comprehensive series of numerical analysis was conducted to assess the impact of BTE airfoil design variables, including trailing-edge thickness and baseline configuration, on the power generation capabilities of the H-type VAWT. The results indicate that an increase in trailing edge thickness correlates with a higher power coefficient at low tip speed ratios (TSRs). When the trailing edge thickness is 3% of the airfoil's chord length, the power coefficient of the vertical axis wind turbine (VAWT) at low tip speed ratios can increase by up to 33.2% compared to the original wind turbine. Additionally, the maximum power efficiency can be improved by 2.94%. Furthermore, the BTE airfoil design, which is achieved by rotating the airfoil's upper and lower surfaces around the leading edge, can result in a more favorable BTE airfoil configuration with respect to its aerodynamic characteristics. The current study reveals that the BTE airfoils present significant potential for urban wind energy utilization, as the reduced operational velocities of BTE airfoils lead to lower noise emissions and heightened safety measures for VAWTs, rendering them an appropriate choice for integration into urban settings.

Article History

Received July 23, 2024
Revised November 4, 2024
Accepted November 21, 2024
Available online February 4, 2025

Keywords:

Blunt trailing edge airfoil
Vertical axis wind turbine
Power coefficient
Numerical simulation

1. INTRODUCTION

Blunt trailing-edge (BTE) airfoils provide multiple structural benefits, and the integration of BTE airfoils allows blade designers to meet structural demands more flexibly without compromising the aerodynamic performance (Sayadi & Shateri, 2013). As VAWTs have advanced, there has been a notable surge in research dedicated to wind turbine airfoils. The primary modification techniques include the direct truncation method (Law, 1987), symmetric thickening method (Standish & Dam, 2003), and the asymmetric thickening and rigid rotation thickening methods (Zhang et al., 2009). Baker et al. (2006) conducted wind tunnel experiments to analyze the aerodynamic performance of symmetric thickened airfoils. They study aimed to assess the influence of varying trailing edge thicknesses on the aerodynamic performance. Zhang and Wei (2013) performed a parametric investigation on asymmetric BTE airfoils and explored the impact of the trailing-edge thickness and its distribution on the aerodynamic performance of wind turbines. Their results revealed that as the trailing-edge thickness increased, the modified airfoil exhibited higher C_d values, and the C_l/C_d ratio initially increased before decreasing. Although a BTE airfoil typically exhibits a higher lift-to-drag ratio compared to a sharp trailing edge airfoil, it also generates more noise. Additionally, the BTE can induce vortex shedding at the trailing edge, which in turn increases drag (Baker et al., 2006; Mayda et al., 2008). Chao and Dam (2007) employed the compressible 3-D RANS method to explore the influence on the aerodynamic performance of modifying the inner section of an NREL Phase VI rotor with a thickened BTE using the S809 airfoil. The results suggest that blade designs incorporating thick and blunt trailing edges could successfully balance structural demands and aerodynamic efficiency in the design of wind turbine rotors. Kumar et al. (2017) conducted both experimental and numerical investigations on the impact of BTE airfoils on VAWTs. They utilized the direct truncation method to increase the thickness of the blunt trailing edge of the NACA0018 airfoils. Furthermore, they explored the effectiveness of reducing wing drag by introducing grooves at the thickened trailing edge of the airfoil. Their study serves as an inspiration for this work, leading to an in-depth analysis of the critical factors associated with BTE airfoils and their influence on the performance of VAWTs. Zhang et al. (2017) investigated the effects of modifying the BTE airfoil on rough-surface airfoils. The results indicated that thickening the BTE modification can significantly reduce power losses. Xu et al. (2017) introduced an active circulation control

NOMENCLATURE

θ	azimuth angle	C_q	power coefficient
ω	angular velocity of blade	C_p	surface pressure coefficient
Δt	time step	C_m	torque coefficient
N	blade number	C_l	lift coefficient
c	blade chord length	C_d	drag coefficient
D	turbine rotor diameter	l_b	ratio of thickness added to the trailing edge of a single airfoil to c
λ (TSR)	tip-speed ratio	l_r	relative thickness
BTE	Blunt Trailing-Edge	VAWT	Vertical Axis Wind Turbine
CFD	Computational Fluid Dynamics	NACA	National Advisory Committee for Aeronautics

technique tailored for thick BTE wind turbine airfoils. Their results demonstrated that employing circulation control on BTE airfoils could yield a notable net energy gain, with circulation control featuring larger groove heights exhibiting superior control efficiency. A study conducted by Zhang et al. (2020) explored the flow characteristics and wind energy utilization of VAWT blades, focusing on their trailing-edge modifications with specific camber profiles. The results demonstrated that increasing the relative camber reduced the areas of positive and negative pressure regions, as well as the wake length and distribution for both the NACA0021 and NACA0021S airfoils concurrently, an increase in wind energy utilization was obtained. Despite the abundance of research on blunt trailing edge (BTE) airfoils, the majority of studies have concentrated on design approach that increase the thickness at the airfoil's trailing edge using the truncation method and with a primary focus on their implementation in horizontal-axis wind turbine blades. Therefore, the integration of blunt trailing edge airfoils into VAWTs merits thorough investigation, given the significant influence that complex dynamic stall characteristics of such airfoil exerts on the overall aerodynamic performance of the turbine (Kumar et al., 2017). Furthermore, the correlation between the airfoil's relative thickness and the thickness of its trailing edge has not been sufficiently explored in existing research.

2. OBJECTIVE OF THE PRESENT WORK

The primary aims of this study is to investigate the aerodynamic performance of the H-Darrieus VAWT with a BTE airfoil using CFD simulations. The effects of critical factors such as the BTE thickness, design method, and baseline configuration of the BTE airfoil are systematically analyzed, these factors have not been fully explored in previous studies. These findings could contribute to a deeper understanding of the aerodynamic properties of the VAWT with BTE airfoil, which holds the potential to increase the generation of urban wind energy through improving the environmental friendliness and operational safety of the conventional VAWT

3. NUMERICAL METHODOLOGY AND VALIDATION

3.1 Geometric Parameters of the Baseline H-Darrieus VAWT

For ease of comparison with the experimental data, the geometric parameters of the entire turbine model are referenced from reference (Raciti Castelli et al., 2010), and the airfoil profile of the VAWT is based on the NACA0021 airfoi as summarized in Table 1. The specific model is shown in Fig. 1 (a).

Table 1 The geometrical parameters of the studied VAWT

Parameters	Numerical value
Rotor diameter D	1.03m
Number of blades N	3
Airfoil	NACA0021
Wind speed	9m/s
Solidity ratio	0.25
Blade chord length c	0.0858m
Height of Blades H	1.456m

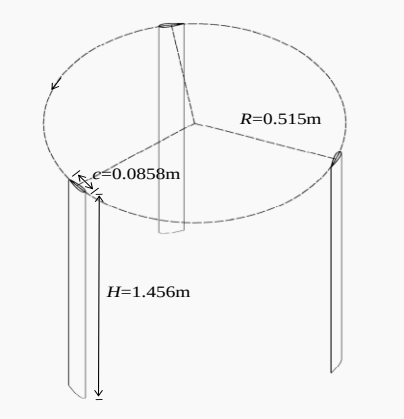

(a)

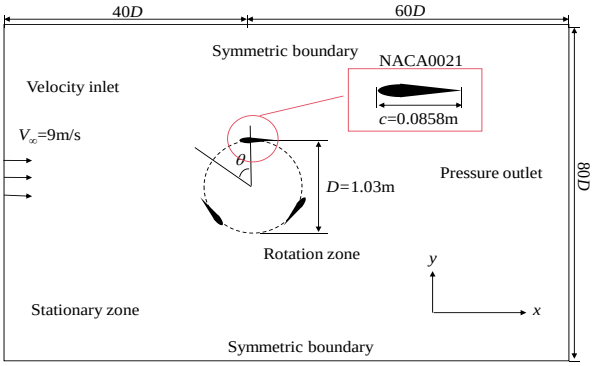

(b)

Fig. 1 Structural models(a) and Schematic of the computational domain for the baseline Darrieus-type straight-bladed VAWT with NACA0021 airfoil blades(b)

3.2 Computational Domain and Grid Generation

URANS models are used in the study, and the governing equations for the conservation of mass and momentum are given below. Here ρ is the density of the fluid, u is the velocity vector field, and t is the time, p is the pressure, τ is the viscous stress tensor, and f represents any external body forces acting on the fluid.

$$\frac{\partial \rho}{\partial t}+\nabla\cdot(\rho \mathrm{u})=0 \tag{1}$$

$$\frac{\partial(\rho \mathrm{u})}{\partial t}+\nabla\cdot(\rho \mathrm{uu})=-\nabla p+\nabla\tau+\rho \mathrm{f} \tag{2}$$

The computation employs a two-dimensional model to simplify the actual VAWT with counterclockwise rotation. The topological structure of the entire computational domain is shown in Fig. 1. The formulas for torque coefficient (C_m) and power coefficient (C_q) are provided below

$$C_m=\frac{M}{\frac{1}{2}\rho_\infty V_\infty^2 AR} \tag{3}$$

$$C_q=\frac{M\omega}{\frac{1}{2}\rho_\infty V_\infty^3 A}=\frac{MR\omega}{\frac{1}{2}\rho_\infty V_\infty^3 AR}=\lambda C_m \tag{4}$$

where M is the total torque, ρ is the flow density, V_∞ is the flow velocity, A is the cross-sectional area R is the rotor radius, and ω is the angular velocity.

The distribution of the computational domain and the mesh on the airfoil surface are shown in Fig. 2. Structured meshes are employed for the airfoil surface. The height of the first layer near the surface is set to 3.0×10^{-5}m to ensure a non-dimensional parameter $y^+\approx1$, and the growth rate is 1.03. A total of 65 inflation layers are established, thereby enhancing the ability of the model to capture of the boundary layer flow on the airfoil surface. The computational domain utilizes structured meshes and is divided into two domains (a rotating and a stationary zone) using a sliding interface. The moving zone consists of the turbine rotor and its movement can be specified through software settings or User-Defined Functions (UDFs) to reproduce the turbine rotation.

3.3 Time-Step Size and Turbulence Model

Fluent 2020 R2 computational fluid dynamics software is used to conduct simulations of the VAWT. The uniform incoming flow velocity V_∞=9 m/s. A sliding mesh model is employed to model the turbine blade rotation, and the turbine is rotated by 0.5° at each time step, thus requiring 720 steps to complete one full revolution. Given the relatively low incoming flow velocity with a Mach number below 0.3, the flow can be treated as incompressible flow (Larose & D'Auteuil, 2008). The pressure-velocity coupling is solved using the SIMPLE algorithm with the second order upwind method.

The formulas for calculating the tip speed ratio (TSR). and time step are provided below, where ω represents the rotational angular velocity, λ denotes the TSR, R is the rotor radius, Δt is the time step, and L corresponds to the arc length associated with a rotation of 0.5°.

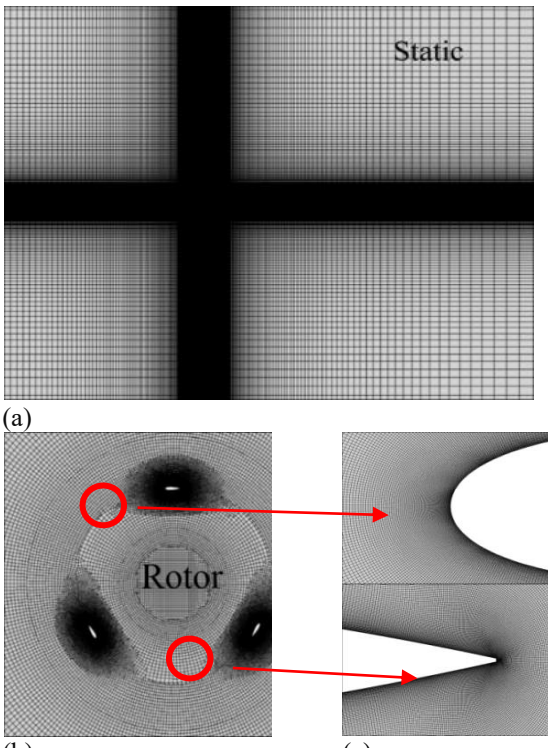

Fig. 2 Details of mesh of arrangement. (a) Overall mesh arrangement. (b) an enlarged view of the rotating region enclosing the single rotor. (c) the close-up views near the airfoil leading and trailing-edge

$$\lambda=\frac{\omega\cdot R}{V_\infty} \tag{5}$$

$$\Delta t=\frac{\omega}{L} \tag{6}$$

Bianchini, Guo and Kumar (Bianchini et al., 2016; Guo et al., 2019; Kumar & Selvaraj, 2023) compared the influence of different turbulence models on the computation results and found that the SST $k-\omega$ model can better simulate flow phenomena induced by pressure gradients, thus providing improved stability and accuracy in numerical computations, particularly for simulations of wind turbines. Hence, this study uses the SST $k-\omega$ turbulence model

3.4 Mesh Independence Study and Model Validation

First, a mesh independence validation is conducted to select an appropriate number of mesh points. Numerical calculations are performed for different mesh densities under the operating condition of λ = 2.64. The average C_m forces on the three blades are listed in Table 2. An appropriate mesh size is chosen to maintain computational accuracy while reducing the computational cost. Therefore 3.4×10^5 mesh points are used for subsequent computations.

Time step validation is conducted under the operating condition of λ = 2.64 with 3.4×10^5 mesh points, as summarized in Table 3. The C_q calculated in this study is obtained by multiplying thet C_m by λ. Therefore C_m is monitored and recorded. Convergence is achieved when

Table 2 The variation of the average torque coefficient with different mesh densities (λ=2.64)

Number of mesh elements	Average C_m of VAWT
2.5E+05	0.138789232
3.4E+05	0.141115714
4.7E+05	0.142565358

Table 3 Results of time step sensitivity study

Time steps (size)	Average C_m of VAWT
T/720	0.140306898
T/1440	0.140557469
T/2160	0.140798444

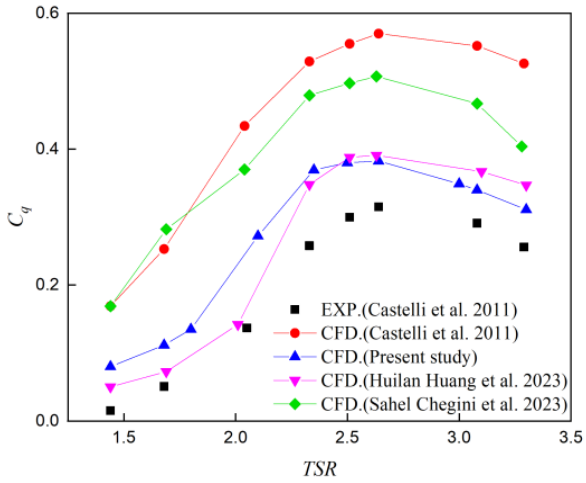

Fig. 3 model validation and comparison with previous studies

the C_m curve shows periodic variations and the difference in the time-averaged C_m (over one turbine revolution) between two successive revolutions is less than 1%. Twenty cycles are computed in this study, and the average C_m of the last three cycles is taken as the computed result. In the Table 3, *T* represents the period.

Based on the validated mesh resolution, the reliability of the numerical algorithm is verified by computing the average C_q at different TSRs. After observing stable cyclic variations at the monitoring points, the computed results are compared with experimental and simulated data from Castelli et al. (Raciti Castelli et al., 2010), Sahel et al. (Chegini et al., 2023), and Huang et al. (2023). The results are shown in Fig. 3.

4. PERFORAMNCE INVESTIGATION OF VAWT WITH BTE AIRFOIL

4.1 Impact of Airfoil Trailing-Edge Thickness

Rigid rotation thickening is a design method proposed by Zhang et al. (2009) that achieves thickening of the airfoil trailing edge by rotating the upper and lower curves of the airfoil around its leading-edge point, as depicted in Fig. 4. In this study, NACA0021 is used as the baseline airfoil configuration. The BTE airfoil generated in this manner is denoted as NACA0021-l_b, where l_b indicates the ratio of the thickness of the BTE of the airfoil to the chord length. This approach

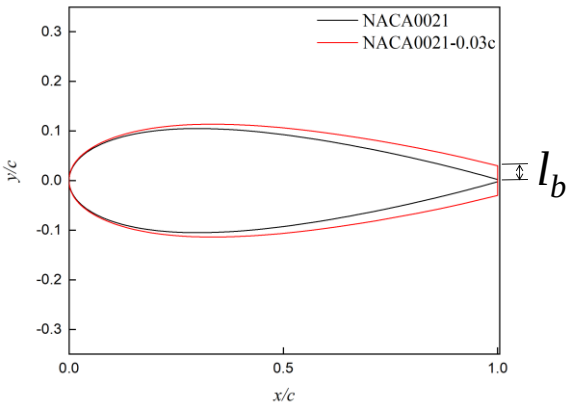

Fig. 4 Schematic representation of the strategy used to increase thickness of airfoil trailing edge through rotational thickening

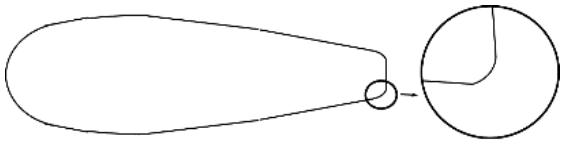

Fig. 5 The BTE airfoil configuration designed with the NACA0021 baseline profile

simultaneously increases the maximum relative thickness of the airfoil. Figure 5 illustrates the resulting BTE airfoil used in the subsequent simulations, in which the rear trailing edge is rounded.

Figures 6(a) illustrates the C_q of the NACA0021 airfoil after thickening by 2%*c*, 3%*c*, 5%*c*, 8%*c*, and 10%*c* using the rigid rotation method (Zhang et al., 2009) at different TSRs. The results show that as the thickness of the airfoil trailing edge increases, the C_q of the VAWT improves at lower TSRs (λ = 1.8) and declines at higher TSRs (λ = 3). With increasing thickness of the airfoil trailing edge, the optimal TSR of the VAWT gradually decreases, whereas the C_q corresponding to the optimal TSR exhibits a trend of initially increasing and then decreasing. At a trailing-edge thickening of 3%*c*, the VAWT achieves its optimal C_q, increasing by 2.94% compared with the original airfoil, with a corresponding optimal TSR of 2.33. At this trailing-edge thickness, the maximum enhancement in C_q reaches 33.2% at a TSR of 2.1. It is observed that at a TSR of 1.8, the NACA0021-0.05c, NACA0021-0.08c, and NACA0021-0.10c airfoils exhibit the greatest enhancements relative to the original airfoil, with improvements of 47.2%, 99.4%, and 124.9%, respectively.

Figure 6(b) and (c) show comparisons of the C_m of the individual blades of the VAWTs with different trailing-edge thicknesses at various TSRs. It is apparent that within the range of phase angles from 90° to 150°, the C_m of the blades increases with an increase in the airfoil trailing-edge thickness. At lower TSRs (λ = 1.8), the VAWT experiences significant flow separation in the downstream region, and the C_m of the blades in this region generally increases with increasing airfoil trailing-edge thickness. As the TSR transitions to higher values (λ=3),

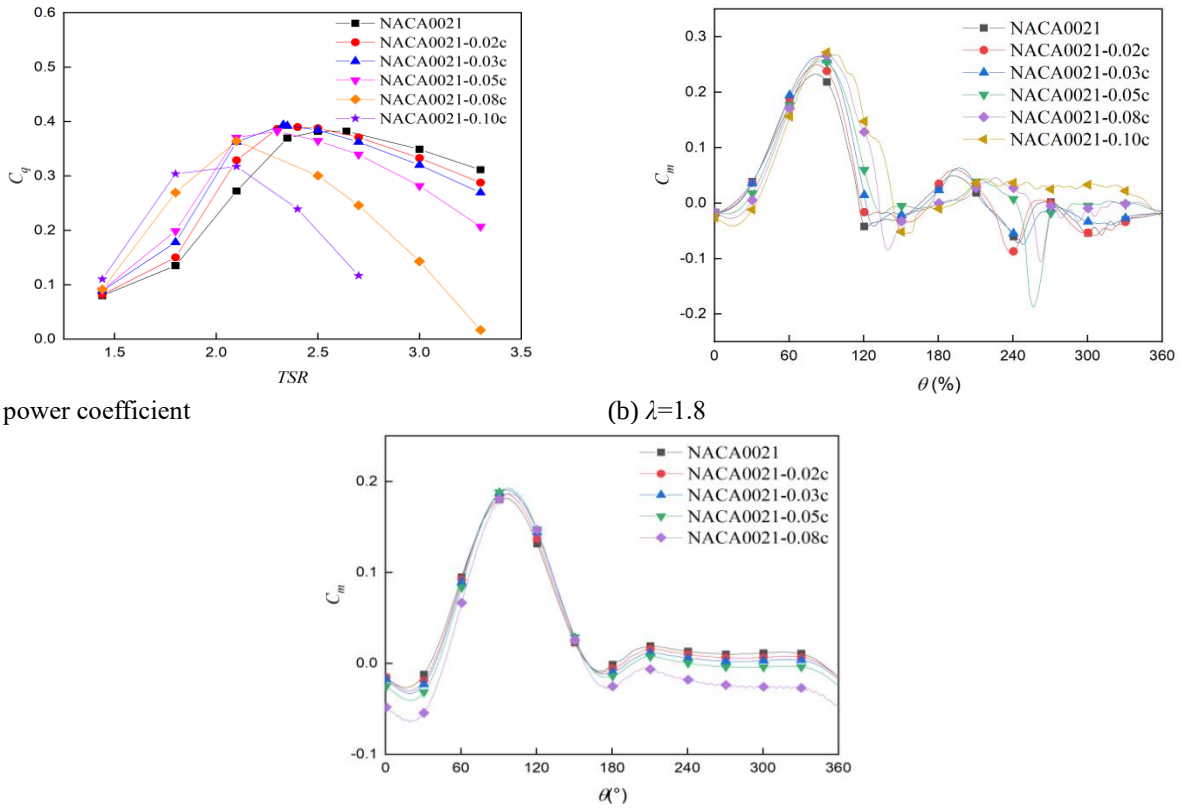

(a) power coefficient (b) λ=1.8

(c) λ=3

Fig. 6 Power coefficients of the VAWTs using BTE airfoils with different trailing edge thicknesses(a) and Comparisons of torque coefficient of a single blade with different trailing edge thickness at three TSRs(b),(c)

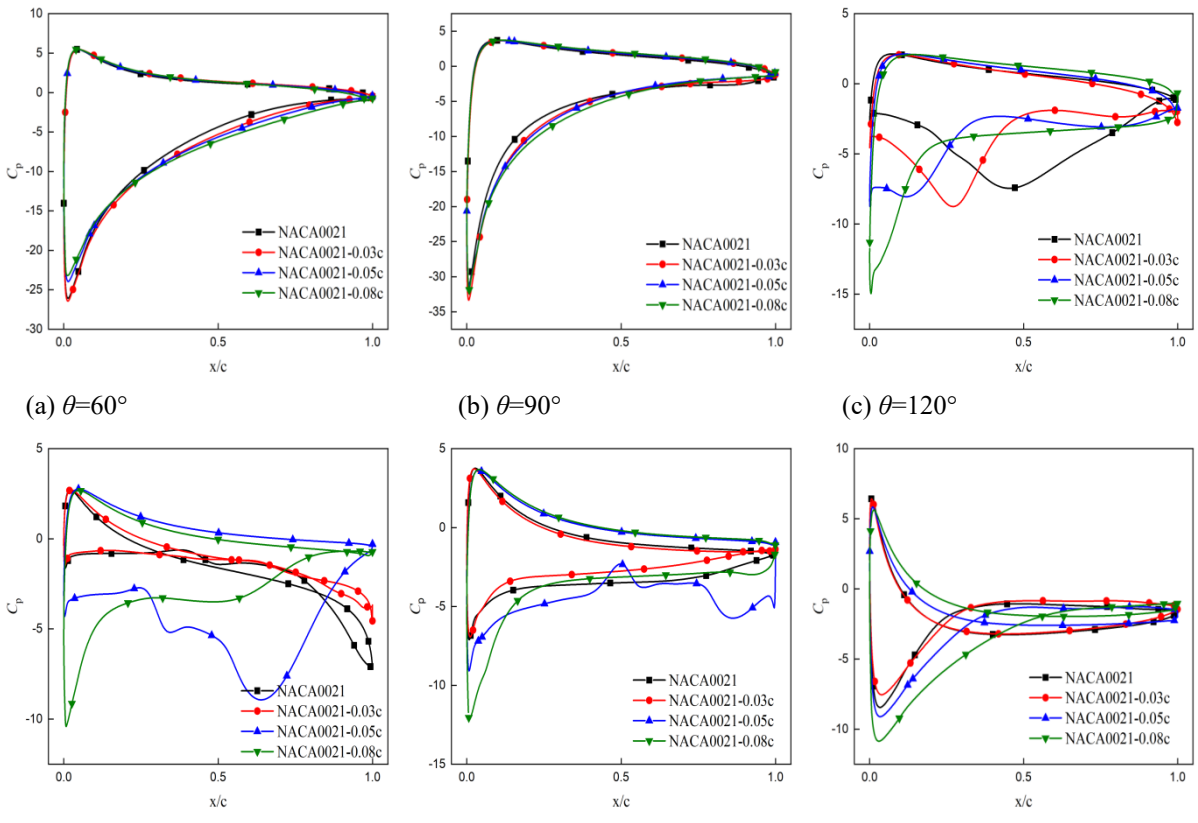

(a) θ=60° (b) θ=90° (c) θ=120°

(d) θ=240° (e) θ=270° (f) θ=330°

Fig. 7 Pressure coefficient distributions around the airfoils with different trailing edge thicknesses at six different azimuthal positions over the revolution (λ=1.8)

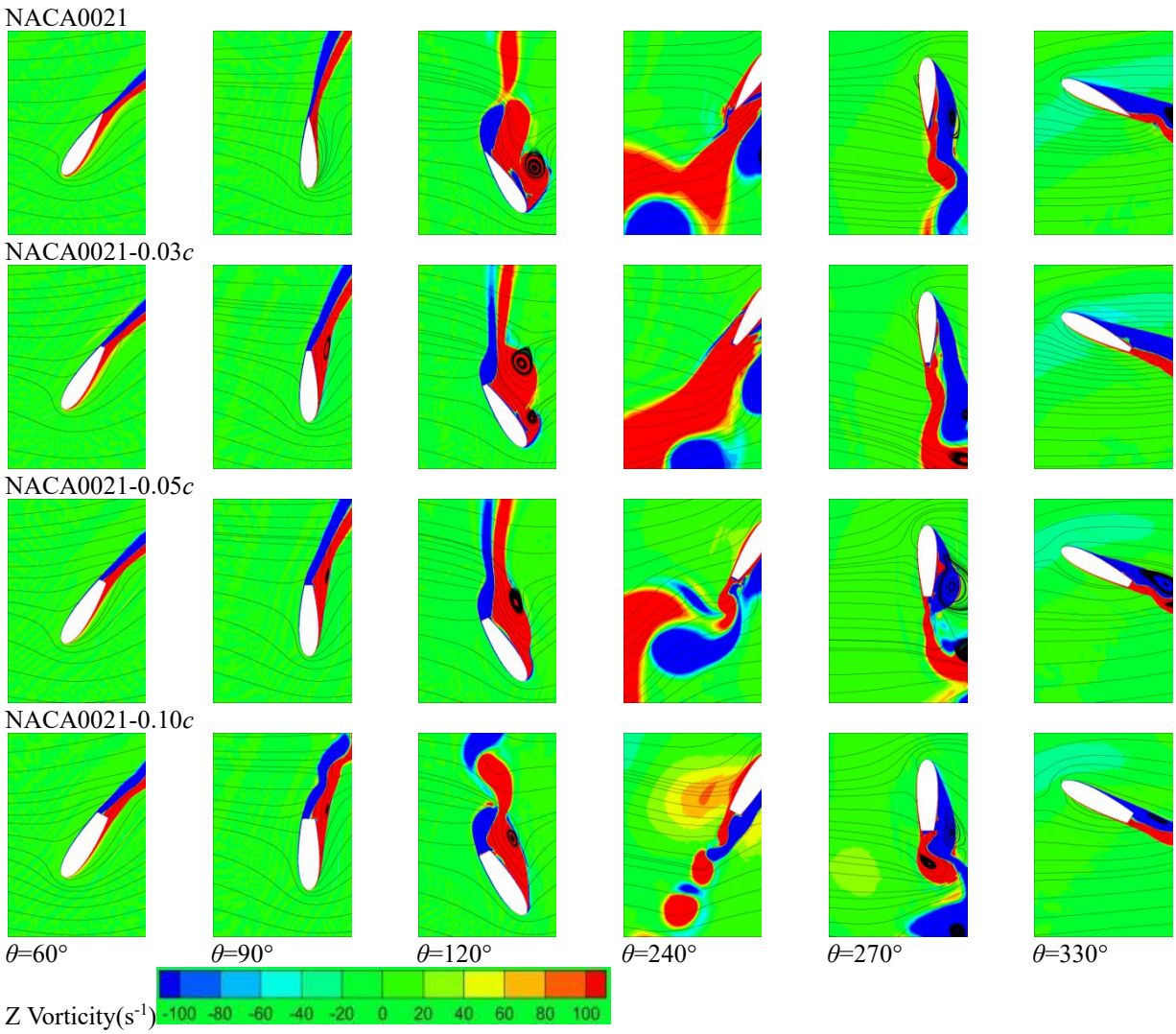

Fig. 8 Vorticity contours around airfoils with different trailing edge thicknesses for six different azimuthal positions in one revolution (λ=1.8)

the extent of the flow separation diminishes. while there is a noticeable decreasing trend in the C_m with increasing blade trailing edge thickness in the downstream region.

To further elucidate the influence of the airfoil trailing-edge thickness on VAWTs, the original airfoil is compared with airfoils having trailing-edge thicknesses of 3%, 5%, and 8%. Figures 7 and 8 show the pressure coefficient (C_p) curves and vorticity contours, respectively, of airfoils with varying trailing edge thicknesses at a TSR of 1.8. As the control of the trailing-edge thickness typically ranges from θ = 40° to 140° and θ = 210° to 360°, phase angles of 60°, 90°, 120°, 240°, 270°, and 330° are chosen for investigation.

From Figs 7 and 8, show that at θ=60°, no flow separation occurs on the airfoil, and there is no significant variation in pressure on the airfoil suction surface. However, the negative pressure peak on the suction surface of the NACA0021-0.05c and NACA0021-0.08c airfoils is reduced compared with that of the other two airfoils. At θ = 90°, no flow separation occurs on the original airfoil, whereas with increasing trailing-edge thickness, flow separation appears on the suction surface. At θ=120°, the airfoil is in a stall condition, and the original airfoil exhibits severe flow separation on its surface. However, with increasing trailing-edge thickness, there is a substantial increase in the negative pressure peak at the leading edge, suppressing the formation and development of leading-edge vortices. The separation point on the airfoil surface moves rearward, and the separation vortices on the suction surface are concentrated toward the mid-rear section of the blade, with a weakening of their intensity. At this juncture, larger trailing-edge thicknesses significantly improve the stall characteristics of the wind turbine blade. At θ=270°, severe flow separation is still observed on the surface of the original airfoil, whereas the NACA0021-0.03*c* airfoil significantly inhibits this flow separation phenomenon, resulting in a minimal pressure difference compared with the other airfoils within this phase angle range. As the thickness of the trailing edge continues to increase, its inhibitory effect on the separation vortices of the airfoil gradually decreases, resulting in an increase in the pressure gradient of the airfoil.

Overall, thicker trailing edges result in more pronounced disturbances at the trailing edge of the airfoil. An increase in the thickness of the trailing edge of the airfoil has a positive effect on the VAWT using this airfoil at this TSR.

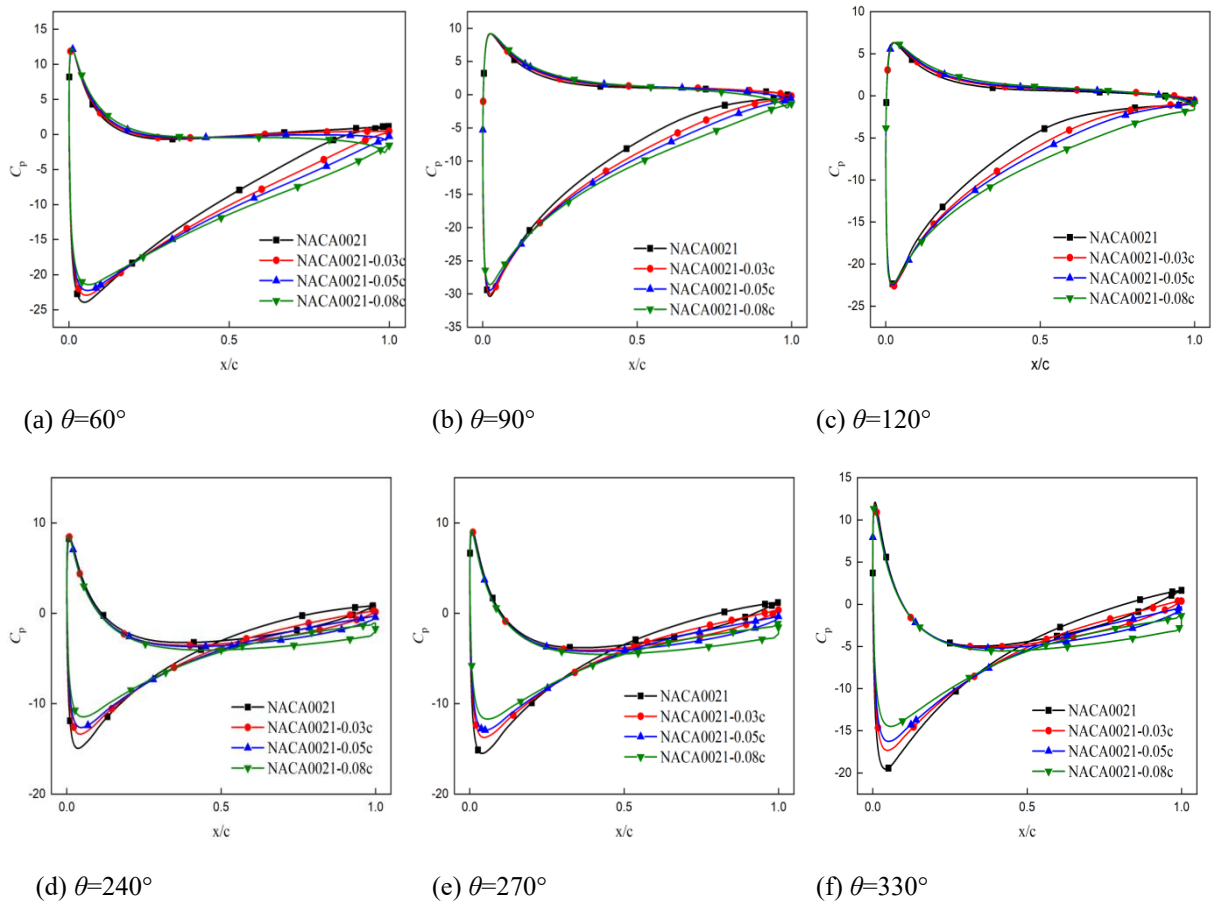

(a) θ=60° (b) θ=90° (c) θ=120°

(d) θ=240° (e) θ=270° (f) θ=330°

Fig. 9 Pressure coefficient distributions around the airfoils with different trailing edge thicknesses at six different azimuthal positions over the revolution (λ=3)

Figure 9 compares the aerodynamic pressure coefficients for individual blades of wind turbines with different trailing-edge thicknesses at λ = 3. Figure 10 presents vorticity contour plots for airfoils with varying trailing-edge thicknesses at different phase angles. As the control of the trailing-edge thickness typically ranges from θ = 40° to 140° and θ = 210° to 360°, phase angles of 60°, 90°, 120°, 240°, 270°, and 330° are selected for investigation.

Overall, Fig. 9 and 10 indicate that the peak negative pressure on the airfoil suction surface decreases with increasing trailing-edge thickness, leading to a reduction in the pressure difference. At this TSR, flow separation typically does not occur on the airfoil surface. However, the NACA0021-0.08c airfoil exhibits vortices at its trailing edge for most phase angles, which is attributed to the structure of its surface. Because of its relatively thick trailing edge, the flow detaches from the airfoil surface at the trailing edge, forming a vortex street. The vortices shed from the airfoil in the upstream region affect the downstream blades. Therefore, although increasing the airfoil trailing-edge thickness enhances the C_q of VAWTs at lower TSRs, it has a pronounced negative effect at higher TSRs.

In general, at this TSR, the C_q of the VAWTs gradually decreases with increasing trailing edge thickness.

Figure 11 compares the drag coefficient curves for airfoils with different thicknesses at two distinct TSRs: λ = 1.8 and λ = 3. Several observations can be made form this figure. First, irrespective of the TSR, the drag coefficient increases with an increase in the airfoil thickness. Second, as the TSR increases, the airfoil's drag coefficient also increases. Finally, at higher TSRs, the drag coefficient curve of the NACA0021-0.08c airfoil exhibits significant fluctuations, which are attributed to the presence of a vortex street resulting from its thicker trailing edge at this TSR.

4.2 Impact of Design Methods of BTE Airfoil

Existing thickening methods include rotational thickening (Zhang et al., 2009) as well as symmetric thickening (Standish & Dam, 2003), asymmetric thickening, and direct truncation (Law, 1987). Owing to the prevalence of symmetric thickening compared with other methods, this study compares rotational thickening with symmetric thickening to explore the impact of different thickening methods on the aerodynamic characteristics of airfoils. In this subsection, we primarily adopt the method proposed by Standish et al. This method ensures a symmetric increase in thickness after the maximum thickness without changing the maximum thickness or centerline distribution of the basic airfoil. The increased thickness is distributed using a power function to ensure smoothness of the modified shape. According to Zhang et al. (2009) the modified coordinates can be represented as follow:

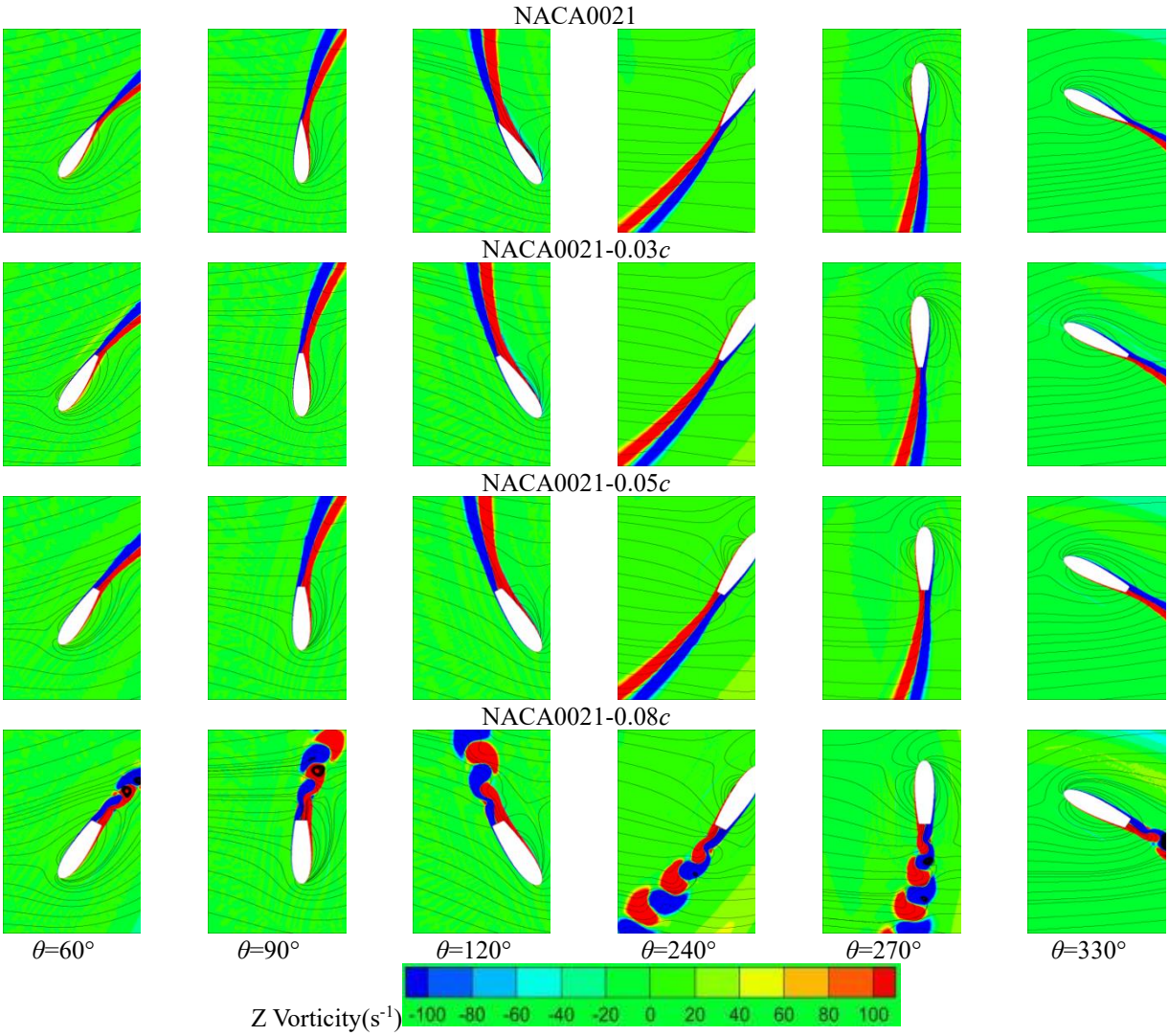

Fig. 10 Vorticity contours around airfoils with different trailing edge thicknesses for six different azimuthal positions in one revolution (=3)

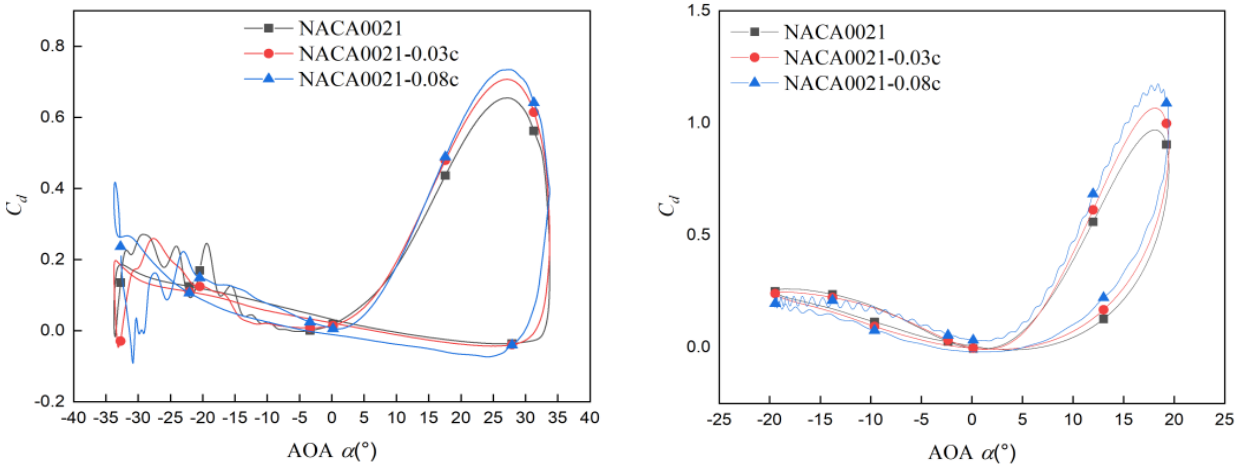

(a) Lift coefficient (b) Drag coefficient

Fig. 11 Comparison of drag coefficients for baseline airfoil and BTE airfoils with trailing edge thicknesses of 0.03*c* and 0.08*c* at two TSRs

$$x = x_0, y = y_0 \pm 0.5\delta\left(\frac{x - x_t}{c - c_t}\right)^n \quad (7)$$

Where δ represents the required increase in trailing edge thickness, and c denotes the geometric chord length of the airfoil. in the table below, t denotes the maximum

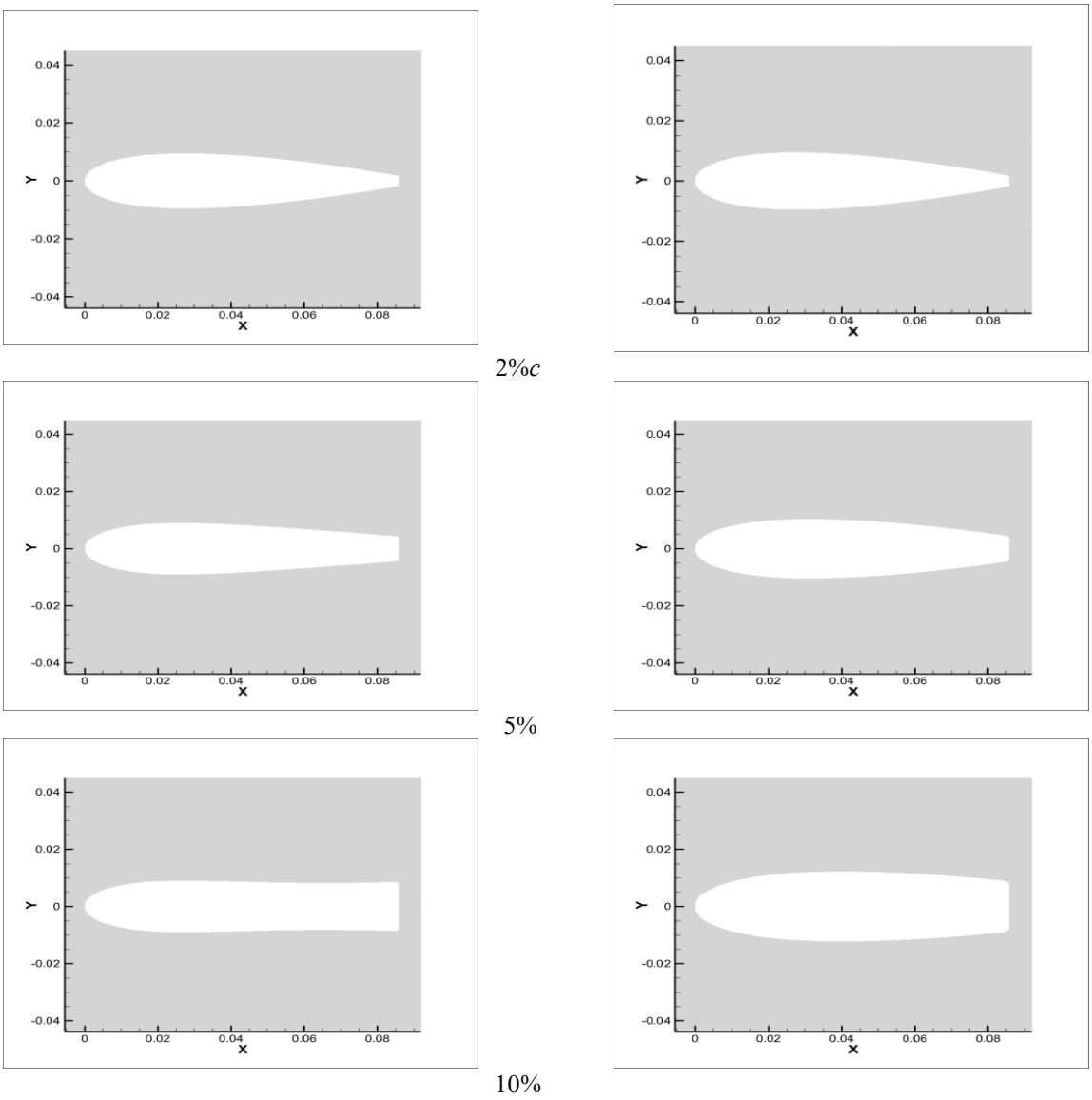

Fig. 12 Plots of the geometric shapes of BTE airfoils designed by two different methods

thickness location, and n is the power-law exponent. As n increases, the modified airfoil profile more closely approaches the original profile. The suitable range for n is typically from 1.8 to 2.5 (Deng et al., 2012), in this subsection, n is set to 2. Symmetrically thickened airfoils are also treated with rounded corners.

Figure 12 compares the geometric shapes of the airfoils obtained using different thickening methods. It is evident that as the thickness increases, the disparity in the geometric profiles of the airfoils obtained by the symmetric and rotational thickening methods gradually increases. The primary reason for this is that the rotational thickening method alters the maximum relative thickness of the airfoil, which increases with the increase in the trailing-edge thickness. When the trailing-edge thickening reaches 10%c, the rotational thickening method yields a maximum relative thickness of 28%c, which represents a 7%c increase compared with the original airfoil.

Figure 13 compares the influence of different thickening methods on the energy efficiency of airfoils utilized in VAWTs. The results show that the overall

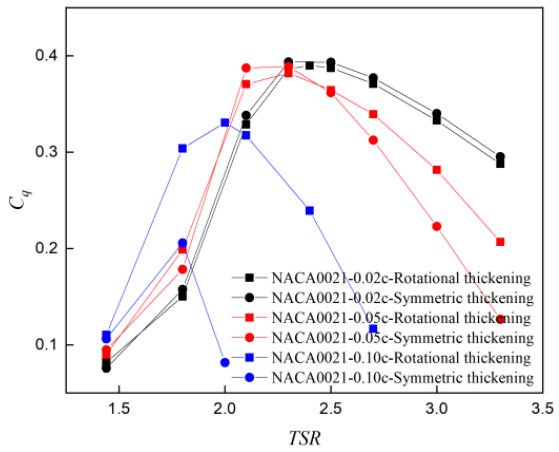

Fig. 13 Power coefficients of the turbines using BTE airfoils obtained by two methods

energy-harvesting efficiency of the VAWTs thickened using the two different methods differs only slightly when the thickness is increased by 2%c. At a thickness of 5%c,

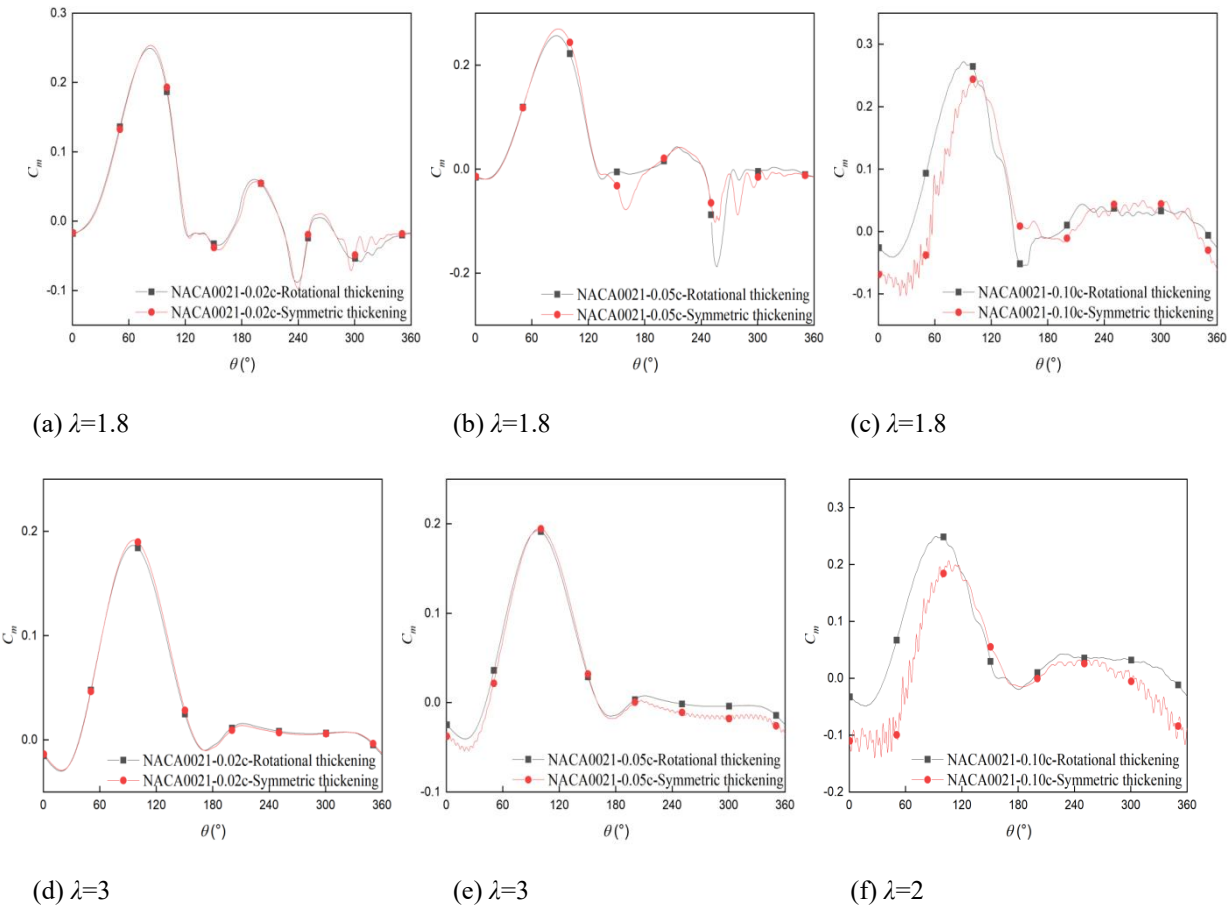

(a) λ=1.8 (b) λ=1.8 (c) λ=1.8

(d) λ=3 (e) λ=3 (f) λ=2

Fig. 14 Comparisons of torque coefficient of a single BTE blade with different trailing edge thickness obtained by two methods

a similar trend is observed, and there is a minimal difference in the energy efficiency between the two methods at low-to-moderate TSRs. However, as the TSR increases, the VAWTs employing airfoils thickened using symmetric thickening exhibit lower energy-harvesting efficiencies than those utilizing airfoils thickened using rotational thickening. This trend becomes more pronounced when the airfoil thickness reaches 10%c. The primary reason for this phenomenon is the alteration of the geometric profile of the airfoil induced by the two thickening methods. When the increase in thickness is relatively small, the differences between the geometric profiles of the airfoils obtained using the two methods are negligible. However, as the thickness increase becomes more substantial, the divergence in the geometric profiles resulting from the two methods becomes increasingly important. This result suggests that airfoils thickened via the rotational thickening method are capable of producing blunt trailing edge profiles with more advantageous aerodynamic properties than those thickened symmetrically. Therefore, the rotational thickening method is then adopted to generate the shape of the BTE airfoil in the subsequent sections of this study, as it seems to be more efficacious.

Figure 14 compares the variation in C_m of a single blade with respect to the phase angle for different thickening methods. Figure 14(a) shows that at λ = 1.8 and a thickness increase of 2%c, the C_m variation curves of the airfoils obtained by the two thickening methods exhibit a high degree of overlap. However, at λ = 1.8 and a thickness increase of 5%c, although the C_m variation curves of the airfoils obtained by both thickening methods still exhibit significant overlap, the differences between the airfoils become increasingly evident compared with a thickness increase of 2%c.

In Fig. 14(c), when λ = 1.8 and the thickness increase is 10%c, this difference becomes particularly pronounced. It can be observed that for θ ranging from 0° to 90°, the C_m of the airfoils thickened by the rotational method are significantly higher than those of the airfoils obtained through symmetric thickening. Moreover, the C_m curve of the airfoils thickened by the rotational method appears much smoother than that of the airfoils obtained through symmetric thickening. The C_m curve of the airfoils obtained through symmetric thickening exhibits noticeable fluctuations when θ ranges from 0° to 90°

Figure 15 compares the vorticity contours for the two different thickening methods applied to airfoils with a thickening of 10%c at λ = 1.8 in VAWTs. Overall, the generation of vortices at the tail of the symmetrically thickened airfoil at this airfoil thickness and TSR is more severe than that of the rotationally thickened airfoil. The generation of these vortices is manifested in the C_m as violent fluctuations in the curve, as shown in Fig. 14(c).

Figure 16 compares the drag coefficients of airfoils obtained through two different thickening methods at λ = 1.8. The results show that the C_d values of the symmetrically thickened airfoils are significantly higher than those of airfoils obtained through rotational

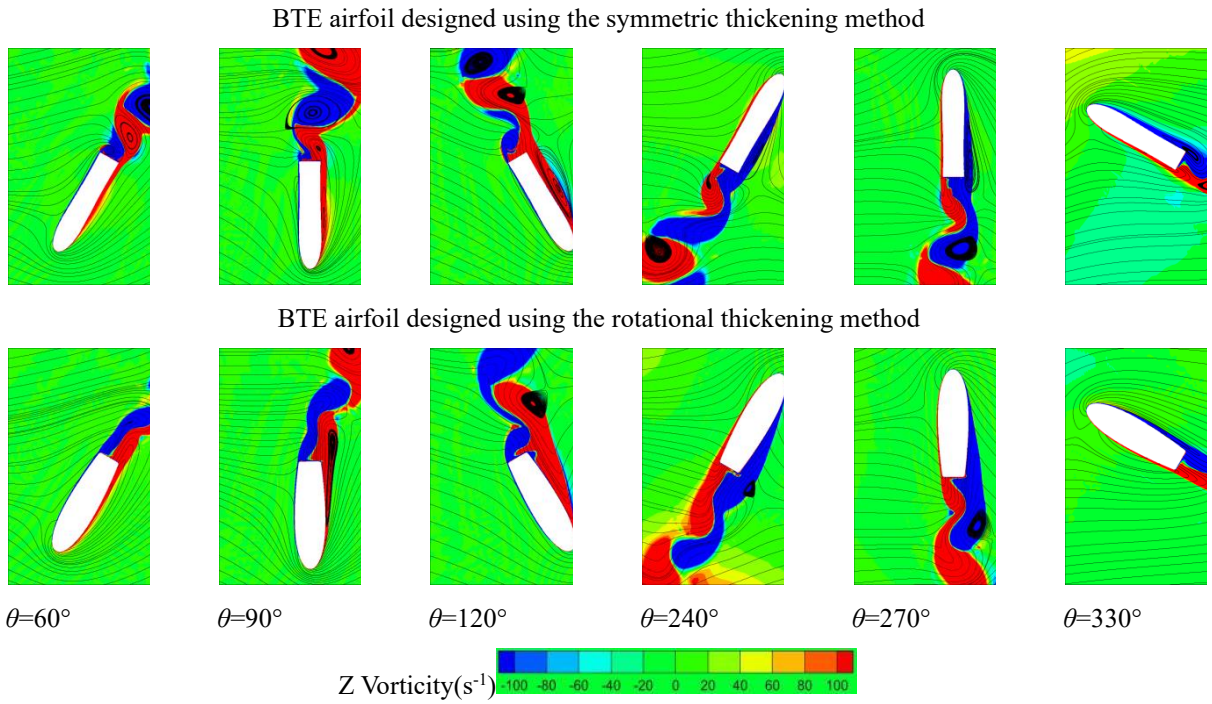

Fig. 15 Vorticity contours around the airfoils with BTE thickness of 0.1*c* obtained by two methods for six different azimuthal positions in one revolution (λ=1.8)

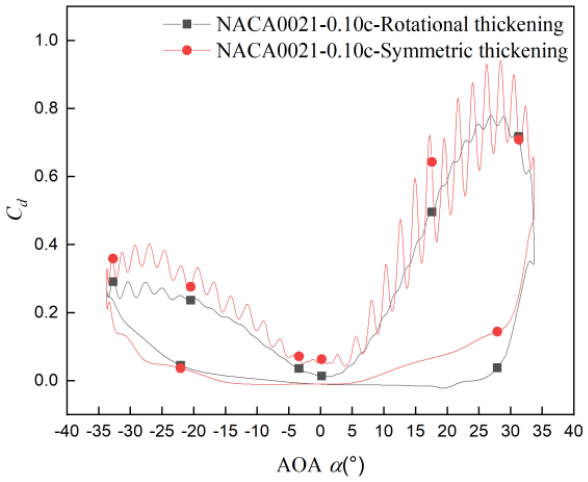

Fig. 16 Comparison of drag coefficients for BTE airfoils with trailing edge thicknesses of 0.1*c* obtained by two methods (λ=1.8)

thickening, and both types of airfoils exhibit fluctuations in C_d owing to the vortex street generated at the trailing edge of the airfoil. The fluctuations in the C_d values of symmetrically thickened airfoils are more pronounced than those of airfoils obtained through rotational thickening, mainly because the generation of vortex streets in symmetrically thickened airfoils is more intense than that in airfoils thickened by rotational means, as evidenced by their vorticity contours.

Figure 17 compares the vorticity contours of airfoils thickened to 5%*c* using two different methods at λ = 3. The symmetrically thickened airfoil exhibits pronounced vortex shedding at the trailing edge, leading to fluctuations in the airfoil C_m, as shown in Fig. 14(e). These vortices increase the drag of the airfoil and also affect the downstream blades in the upwind region of the VAWT, further increasing the drag. This ultimately reduces the energy-harvesting efficiency of the VAWT.

Figure 18 compares the vorticity contours of airfoils thickened to 10% using two different methods at λ = 2. Combined with Fig. 14(f), both thickening methods result in vortex shedding at the trailing edge of the airfoil, however, the vortex shedding from the symmetric thickening method is notably more intense. Although rotational thickening also induces vortex shedding at the trailing edge of the airfoil, this phenomenon occurs with a larger airfoil thickness than under symmetric thickening. Additionally, under the same TSR, the vortex-shedding phenomenon in airfoils thickened by the rotational method is less severe compared with that in airfoils thickened symmetrically.

The C_m curves obtained at greater thicknesses and the energy-harvesting efficiency achieved by these airfoils in the VAWT indicate that rotational thickening is superior to symmetric thickening when the thickness is increased significantly.

4.3 Impact of Initial Baseline Airfoil Geometry

Because the rotational thickening method not only alters the trailing-edge thickness of the airfoil but also affects its relative thickness, this subsection investigates the impact of BTE thickening on airfoils with different thicknesses. The study NACA0012, NACA0015, NACA0018, and NACA0021 airfoil profiles with a thickness of 3%*c* are compared. Using the rotational thickening method, the actual relative thickness of the thickened airfoils increases by approximately 2%*c*. Specifically, the actual relative thicknesses of NACA0012 NACA0015 NACA0018 and NACA0021 become 14%*c*, 17%*c*, 20c%*c*, and 23%*c*, respectively.

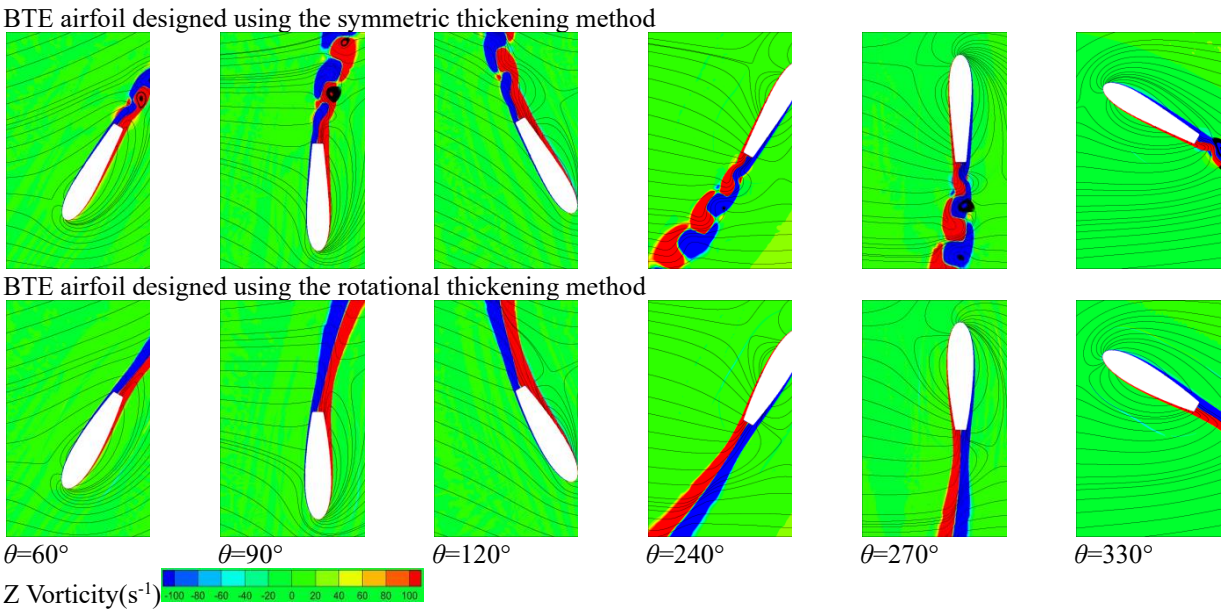

Fig. 17 Vorticity contours around the airfoils with BTE thickness of 0.05c obtained by two methods for six different azimuthal positions in one revolution (λ=3)

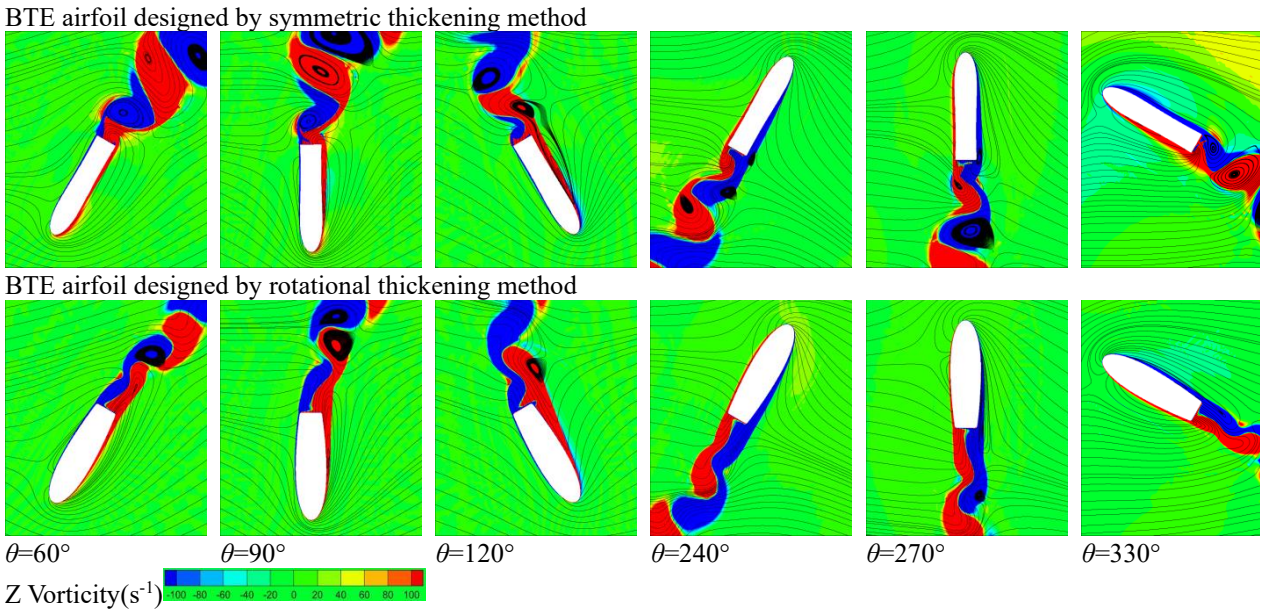

Fig. 18 Vorticity contours around the airfoils with BTE thickness of 0.1c obtained by two methods for six different azimuthal positions in one revolution (λ=2)

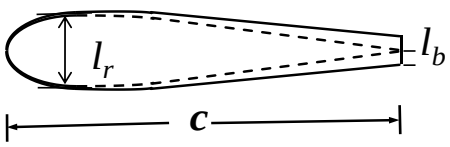

Fig. 19 The schematic of relative thicknesses of the BTE airfoil

Because this subsection focuses on the relative thickness parameter, the variation in the actual relative thickness of the airfoil profiles does not have a substantive impact on the conclusions. The naming convention for the airfoils after trailing-edge thickening remains consistent with the relative thickness of the original airfoil plus the trailing-edge thickness, e.g., NACA0012-0.03*c*, NACA0015-0.03*c*, NACA0018-0.03*c*, and NACA0021-0.03*c*. Figure 19 shows a schematic of the thickness and relative thickness of the trailing edge. Because it is necessary to investigate the relationship between the relative thickness and airfoil trailing-edge thickness, the ratio of l_r to l_b is defined as Rt (the relative trailing-edge thickness).

Hence,

$$Rt = \frac{l_r}{l_b} \tag{8}$$

In the above equation, l_r is the maximum relative thickness of the original airfoil based on which the BTE airfoil is designed, and l_b is the thickness added to the trailing edge of the airfoil. In terms of the actual relative thickness of the airfoil, the Rt values for four different

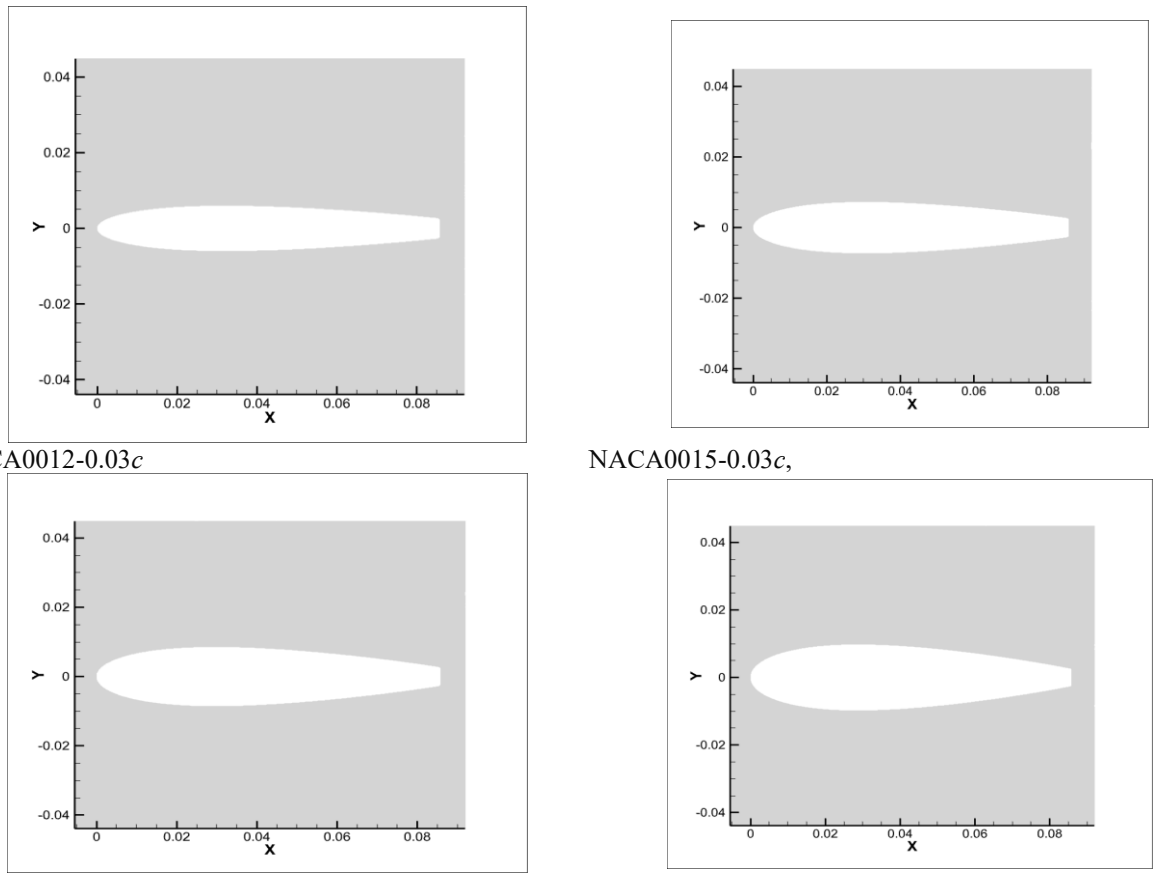

NACA0012-0.03*c* NACA0015-0.03*c*,

NACA0018-0.03*c* NACA0021-0.03*c*

Fig. 20 Plots of the BTE airfoils designed based on different baseline airfoil configurations for a given trailing edge thickness of 3%*c*

relative thicknesses are as follows: $Rt_{\text{NACA0012-0.03c}}$=4.67, $Rt_{\text{NACA0015-0.03c}}$=5.67, $Rt_{\text{NACA0018-0.03c}}$=6.67 and $Rt_{\text{NACA0021-0.03c}}$=7.67.

Figure 20 compares the geometric shapes of airfoils with different Rt values.

Figure 21(a) illustrates the C_q of VAWTs with airfoil Rt value at different TSRs. The results show that at a low TSRs (λ = 1.8), the greater the *Rt* value of the airfoil, the higher C_q of the VAWT. However, at moderate (λ=2.5) and high (λ=3) TSRs, the VAWT achieves optimal C_q when the *Rt*=5.67. As the airfoil *Rt* increases, the C_q of the VAWT gradually decreases.

Figure 21(b) and (c) presents a comparative graph of the C_m of individual airfoils at different TSRs. From the graph, it can be observed that at λ=1.8, within the range of θ=0°~120°, the C_m of the airfoil increases with increasing *Rt* value of the airfoil. At λ=3, within the range of θ=0°~120°, there is minimal difference in the C_m of the four airfoils with different *Rt,* and the C_m of the NACA0015-0.03*c* airfoil remains the highest. Under this TSR, when the airfoil is in the downstream region of the VAWT, the C_m curve of the NACA0012-0.03*c* airfoil exhibits noticeable minor fluctuations. This is because as the *Rt* value of the airfoil decreases, the thickness of the airfoil's trailing edge becomes closer to the relative thickness of the airfoil itself. At high aspect ratios, the presence of a vortex street phenomenon becomes more pronounced at the airfoil's trailing edge, resulting in such fluctuations.

Figure 22 illustrates the pressure coefficient curves for airfoils with different Rt at λ = 1.8. As the control of trailing-edge thickness typically ranges from θ = 60°~330°, phase angles of 60°, 90°, 120°, 240°, 270°, and 330° are selected for investigation. Siddhant et al. (Jain & Saha, 2020) noted that, for Darrieus-type turbines with thin airfoils, a smaller leading-edge radius is disadvantageous for airflow passage, leading to the formation of separation vortices at the leading-edge point, thus resulting in leading-edge stall. For thicker airfoils, the development process of the dynamic stall on the blades changes, with flow separation on the blade surface starting from the trailing edge and exhibiting trailing-edge stall characteristics.

Figures 22 shows that at θ = 60°, as the relative thickness of the airfoil increases, the negative pressure peak on the suction surface gradually decreases, and the pressure gradient also decreases. At θ = 90°, flow separation occurs at the leading edge of the NACA0012-0.03*c* airfoil, as the relative thickness of the airfoil increases, the separation point on the surface moves backward. Because the maximum relative thickness of the NACA0012-0.03c airfoil is the smallest, the influence of the trailing edge is greater under the same trailing-edge thickness of 3%*c*, leading to a decrease in the negative pressure peak on the suction surface. At θ = 240°, all of the airfoils are in the stall conditions. At θ = 270°, the NACA0012-0.03*c* airfoil exhibits stranger vorticity on its suction surface than the other airfoils, resulting in a larger negative pressure peak and pressure gradient.

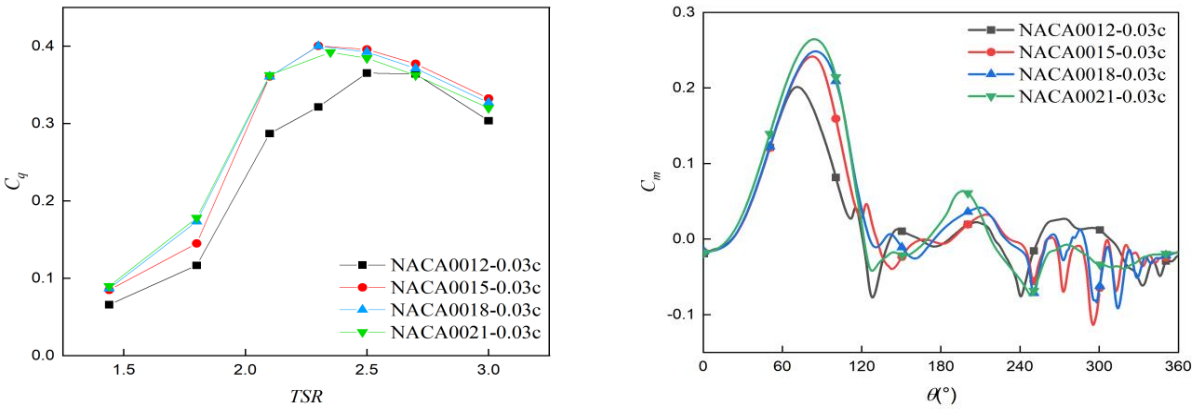

(a) power coefficient (b) λ=1.8

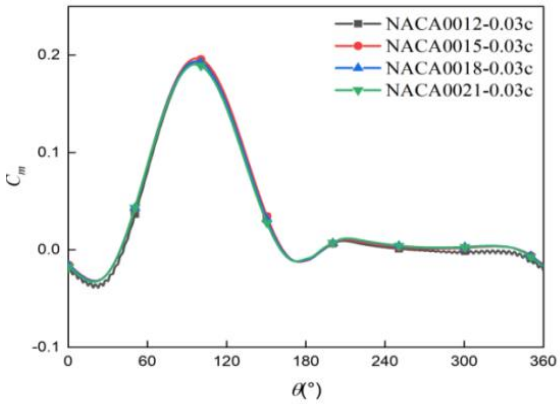

(a) λ=3

Fig. 21 Power coefficients of the turbines using BTE airfoils with different relative thicknesses for a given trailing edge thickness of 3%*c* (a) and comparisons of torque coefficients of a single BTE blade with different relative thickness at two TSRs (b)&(c)

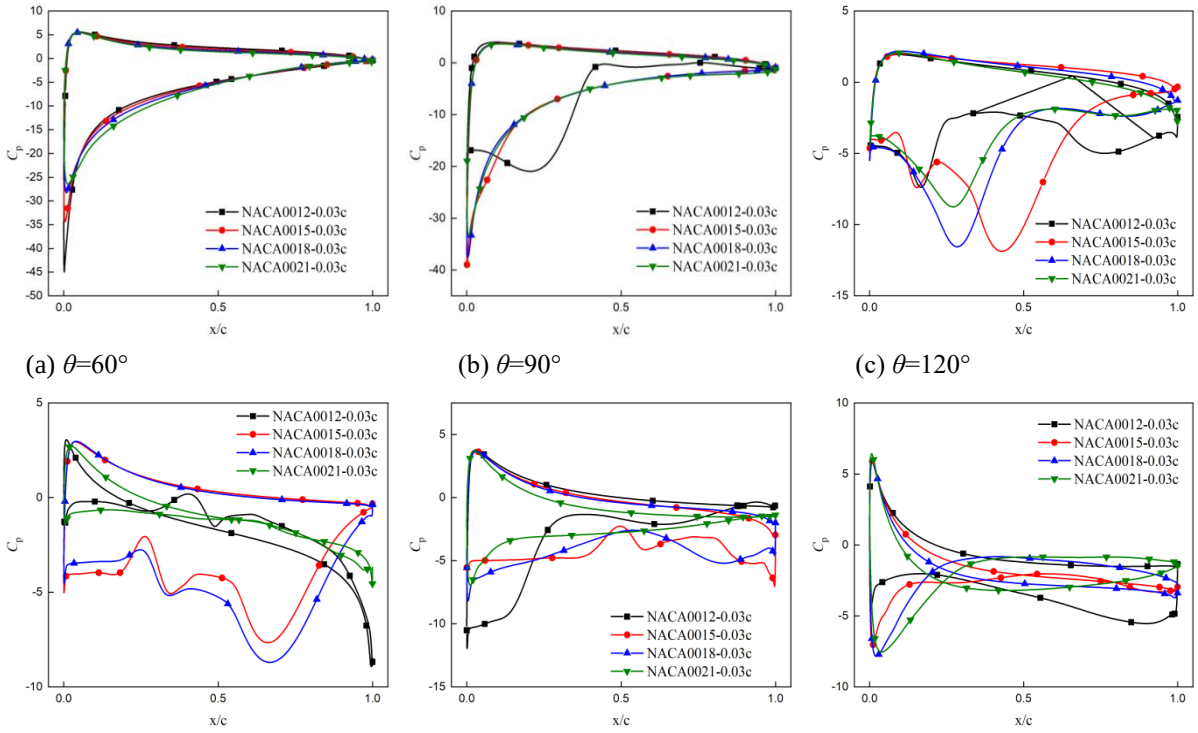

(a) θ=60° (b) θ=90° (c) θ=120°

(d) θ=240° (e) θ=270° (f) θ=330°

Fig. 22 Pressure coefficient distributions around the BTE airfoils with different relative thicknesses for a given trailing edge thickness of 0.03*c* at six different azimuthal positions over the revolution (λ=1.8)

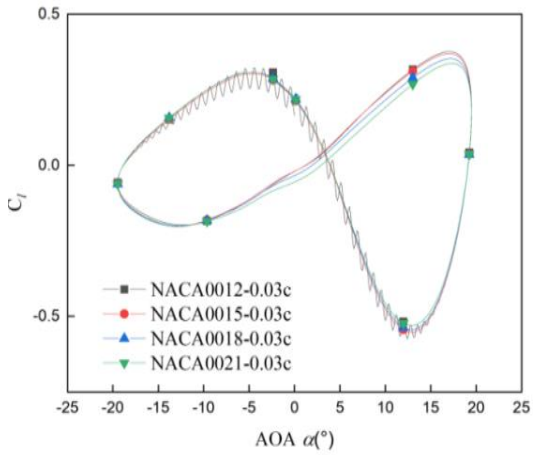

(a) Lift coefficient

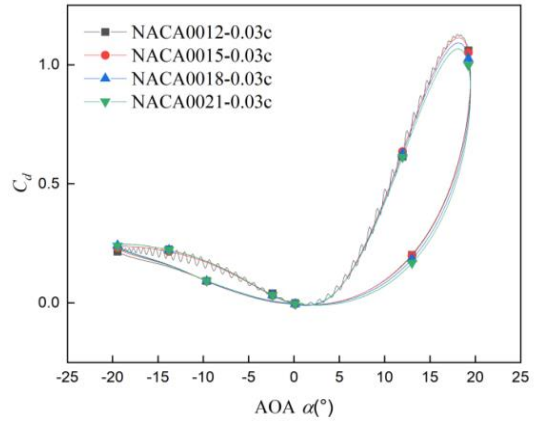

(b) Drag coefficient

Fig. 23 Comparison of lift and drag coefficients for BTE airfoils with different relative thickness for a given trailing edge thicknesses of 0.03*c* (λ=3)

Figure 23 compares C_l and C_d for airfoils with different *Rt* at λ = 3. At λ=3, both C_l and C_d decrease as the *Rt* value of the airfoil increases. However, when *Rt* is extremely small, vortex shedding occurs at the trailing edge of the airfoil at high aspect ratios. Combining this observation with Fig. 22(a), it can be inferred that at lower aspect ratios, higher *Rt* values correspond to better C_q for VAWTs. Conversely, smaller *Rt* values at high aspect ratios have a positive effect on the energy harvesting of VAWTs. However, when *Rt* is excessively small, vortex shedding occurs, which significantly reduces the energy harvesting efficiency of VAWTs.

5. CONCLUSIONS

In this study, the aerodynamic characteristics of an H-Darrieus VAWT with the a BTE airfoil are comprehensively analyzed using CFD simulations. The effects of several critical factors (including the BTE thickness, design method of the BTE airfoil, and baseline airfoil configuration) on the performance of the H-Darrieus VAWT are then studied. Our results suggest that the BTE airfoil can significantly improve the aerodynamic performance of an H-Darrieus VAWT at low TSRs Moreover, a the higher maximum C_P can also be achieved at a smaller optimal TSR compared with the conventional counterpart, indicating its promising application for wind energy exploitation in dense urban areas owing to its advantages of a relatively low noise level and high operational safety. The major results of this study can be summarized as follows:

(1) For the three-bladed VAWT with NACA0021 BTE airfoil, its power coefficient is notably higher at low TSRs than conventional VAWTs with sharp trailing edge airfoil. However, the operating range of the VAWT with BTE airfoil is narrower and becomes increasingly so with greater BTE thickness.

(2) When the BTE airfoil's trailing edge thickness is 3%, 5%, 8%, and 10% of its chord length, the maximum increase in the wind turbine's power coefficient can reach 33.2%, 47.2%, 99.4%, and 124.9%, respectively.

(3) When the trailing edge thickness is small, there's no notable difference in performance between VAWTs with BTE airfoils made by rigid rotation or symmetric thickening. However, with greater thickness, significant performance variations occur, with the rigid rotation method showing superior results.

(4) For airfoils with a 3%*c* trailing edge thickness, thicker airfoils (NACA0015, NACA0018, NACA0021) are more suitable than the thin airfoil (NACA0012) as a baseline for BTE airfoils, offering better aerodynamic performance on H-Darrieus VAWTs.

Further research needs to explore possible flow control techniques like active blade pitch control to increase power capture of the H-Darrieus VAWT with the BTE airfoil at high TSRs. Moreover, the self-starting aerodynamic characteristics of the VAWT with the BTE airfoil are also worthy of additional investigations.

ACKNOWLEDGEMENTS

This work was supported by National Natural Science Foundation of China (no. 52176194).

CONFLICT OF INTEREST

The authors have no conflict interests to disclose

AUTHORS CONTRIBUTION

Zhenyu Kong: Investigation, writing-Original Draft
Xiaojing Sun: Supervision, Writing-Review & Editing

REFERENCE

Baker, J. P., Mayda, E. A., & Dam, C. P. V. (2006). Experimental analysis of thick blunt trailing-edge wind turbine airfoils. *Journal of Solar Energy Engineering,* (4), 128. https://doi.org/10.1115/1.2346701

Bianchini, A., Balduzzi, F., Ferrari, L., Ferrara, G., & Maleci, R. (2016). Critical issues in the CFD simulation of Darrieus wind turbines. *Renewable Energy*, *85*, 419-435. https://doi.org/10.1016/j.renene.2015.06.048

Chao, D. D., & Dam, C. P. V. (2007). Computational aerodynamic analysis of a blunt trailing-edge airfoil modification to the NREL phase VI rotor. *Wind Energy*, *10*(6), 529-550.

https://doi.org/10.1002/we.239

Chegini, S., Asadbeigi, M., Ghafoorian, F., & Mehrpooya, M. (2023). An investigation into the self-starting of darrieus-savonius hybrid wind turbine and performance enhancement through innovative deflectors: A CFD approach. *Ocean Engineering*. https://doi.org/10.1016/j.oceaneng.2023.115910

Deng, L., Qiao, Z., & Yang, X. (2012). Aerodynamics performance computational of trailing-edge-blunting methods of flatback airfoil for large wind turbine based on rans equation. *Acta Energiae Solaris Sinica*, *33*(4), 545-551. https://doi.org/10.3969/j.issn.0254-0096.2012.04.004

Guo, Y., Li, X., Sun, L., Gao, Y., Gao, Z., & Chen, L. (2019). Aerodynamic analysis of a step adjustment method for blade pitch of a VAWT. *Journal of Wind Engineering and Industrial Aerodynamics*, *188*, 90-101. https://doi.org/10.1016/j.jweia.2019.02.023

Huang, H., Nong, Z., Li, G., & Li, J. (2023). Research and optimization of a built-in entity vertical axis wind turbine by variable pitch strategy. *Journal of Building Engineering*. https://doi.org/10.1016/j.jobe.2022.105810

Jain, S., & Saha, U. K. (2020). On the influence of blade thickness-to-chord ratio on dynamic stall phenomenon in H-type Darrieus wind rotors. *Energy Conversion and Management*, *218*, 113024. https://doi.org/10.1016/j.enconman.2020.113024

Kumar, K. R., & Selvaraj, M. (2023). Novel deep learning model for predicting wind velocity and power estimation in advanced INVELOX wind turbines. *Journal of Applied Fluid Mechanics*. https://doi.org/10.47176/jafm,16.06.1637

Kumar, P. M., Kulkarni, R., Srikanth, N., & Lim, T. C. (2017). Performance assessment of darrieus turbine with modified trailing edge airfoil for low wind speeds. *Smart Gird and Renewable Energy, 8*(12), 425-439. https://doi.org/10.4236/sgre.2017.812028

Larose, G. L., & D'Auteuil, A. (2008). Effect of local air compressibility on the aerodynamics of rectangular prisms at Mach number below 0.3. BBAA VI *International Colloquium on: Bluff Bodies Aerodynamics & Applications. Milano*, Italy, July,

Law, S. P. G., G. M. (1987). *Wind tunnel evaluation of a truncated NACA 64-621 airfoil for wind turbine applications.* Final Report Ohio State Univ Columbus. *https://doi.org/10.2172/6443460*

Mayda, E. A., Van Dam, C. P., Chao, D. D., & Berg, D. E. (2008). Flatback airfoil wind tunnel experiment. *Airfoils*, 151-162. http://doi.org/10.2172/933221

Raciti Castelli, M., Ardizzon, G., Battisti, L., Benini, E., & Pavesi, G. (2010). *Modeling strategy and numerical validation for a darrieus vertical axis micro-wind turbine.* ASME 2010 International Mechanical Engineering Congress and Exposition. https://doi.org/10.1115/imece2010-39548

Sayadi, H., & Shateri, A. R. (2013). Numerical simulation of turbulent flow around an airfoil with blunt trailing edge aerodynamic characteristics modification of this airfoil with base and aerodynamic cavity. *International Journal of Advanced Design & Manufacturing Technology*, *6*(1), 61-67. https://www.semanticscholar.org/paper/Numerical-Simulation-of-Turbulent-Flow-around-an-Sayadi-Shateri/db89ad46d949025c2d8e06a13f5fd7a99be875af

Standish, K., & Dam, C. P. V. (2003). Aerodynamic analysis of blunt trailing edge airfoils. *Journal of Solar Energy Engineering-transactions of The Asme*, *125*, 479-487. https://doi.org/10.1115/1.1629103

Xu, H. Y., Qiao, C. L., Huiqiang, Y., & Ye, Z. (2017). Active Circulation control on the blunt trailing edge wind turbine airfoil. *AIAA Journal*, *56*, 554-570. https://doi.org/10.2514/1.J056223

Zhang, L., Yang, K., Zhao, X., & Xu, J. (2009). Aerodynamic Influence of different trailing-edge changing methods to the blunt brailing-edge aurfoil. *Journal of Engineering Thermophysics*. https://doi.org/:10.3321/j.issn:0253-231X.2009.05.014

Zhang, X., Li, Z., Yu, X., & Li, W. (2020). Aerodynamic performance of trailing-edge modification of H-Type VAWT Blade considering camber effect. *International Journal of Aeronautical and Space Sciences,* (3), 21. https://doi.org/10.1007/s42405-019-00241-x

Zhang, X., Wang, G., Zhang, M., Liu, H., & Li, W. (2017). Numerical study of the aerodynamic performance of blunt trailing-edge airfoil considering the sensitive roughness height. *International Journal of Hydrogen Energy*, *42*(29), 18252-18262. https://doi.org/10.1016/j.ijhydene.2017.04.158

Zhang, X., & Wei, L. (2013). Effect of asymmetric blunt trailing-edge thickness on aerodynamic performance of wind turbine airfoils. *Zhongguo Dianji Gongcheng Xuebao/Proceedings of the Chinese Society of Electrical Engineering*, *33*(14), 107-113. https://doi.org/10.13334/j.0258-8013.pcsee.2013.14.014